Impact of Motor Stator Winding Faults on Motor Differential-mode Impedance and Mode Transformation

Fei Fan[1], *Zhenyu Zhao*[1*], *Huamin Jie*[1], *Quqin Sun*[2], *Pengfei Tu*[1], *Zhou Shu*[1], *Wensong Wang*[1] *and Kye Yak See*[1]

(1. School of Electrical and Electronic Engineering, Nanyang Technological University, Singapore 639798, Singapore;
2. Science and Technology on Thermal Energy and Power Laboratory, Wuhan Second Ship Design and Research Institute, Wuhan 430000, China)

Abstract: Motor impedance and mode transformation have significant effects on the electromagnetic interference (EMI) generated in motor drive systems. Stator winding faults commonly cause motor failure; however, in their early stages, they may not affect the short-term operation of the motor. To date, EMI noise under the influence of premature stator winding faults has not been adequately studied, particularly the differential-mode (DM) noise due to the common-mode (CM)-to-DM transformation. This study investigates and quantifies the influence of stator winding faults on the motor DM impedance and mode transformation. First, the transmission line model of an induction motor is described based on the scattering (*S*) parameter measurements of each phase of the motor. It offers the flexibility to emulate different types of stator winding faults at specific locations and various severities, such that the impacts of the faults on the motor DM impedance can be easily estimated. Second, a test setup is proposed to quantify the CM-to-DM transformation due to the stator winding faults. The findings of this study reveal that even the early stages of stator winding faults can result in significant changes in the DM noise.

Keywords: Differential-mode (DM) impedance, DM noise, mode transformation, motor stator winding faults, transmission line model

1 Introduction

High-frequency pulse width modulation (PWM) inverters have been widely adopted in motor drive systems because of their high power conversion efficiency, flexible speed control, and competitive pricing [1-4]. However, high-speed switching operations generate conducted emissions that can cause potential problems involving electromagnetic interference (EMI) [5-10]. These undesirable emissions can be in either differential mode (DM) or common mode (CM). Although EMI noise characteristics and corresponding mitigation techniques for motor drive systems have been extensively studied [11-15], the impact of stator winding faults on EMI noise emissions has not been investigated in detail. Stator winding faults have been reported to affect the CM noise emission, but no further studies have been conducted on the conversion of CM-to-DM noise emission [16].

Stator winding faults account for approximately 40% of the total faults in induction motors [17], and they are mainly classified into three categories: turn-to-turn, phase-to-phase, and phase-to-ground faults [18]. The motor drive system continues to operate when a stator winding fault occurs in its initial state, particularly in a highly reliable insulated terrestrial system [19]. The CM-to-DM conversion due to stator winding faults can increase the DM noise emission, and the impact of this conversion has yet to be well studied and quantified.

Fig. 1 shows a typical three-phase motor drive

Manuscript received May 15, 2022; revised July 10, 2022; accepted August 8, 2022. Date of publication September 30, 2022; date of current version September 2, 2022.

* Corresponding Author, E-mail: zhao0245@e.ntu.edu.sg

Digital Object Identifier: 10.23919/CJEE.2022.000022

system in which the DM emission flows through one of the phases to the induction motor and returns via the other two phases to the direct-current (DC) link capacitor of the power source. The DC link serves as a low-AC impedance path between the DC rails, which decouples the DM currents at the input and output sides of the inverter [20]. Therefore, the inverter can be represented as a DM noise source, whereas the induction motor can be treated as a DM noise termination source. Considering that a stator winding fault can affect the DM impedance and CM-to-DM transformation of the induction motor, this study investigates and quantifies these effects on DM noise.

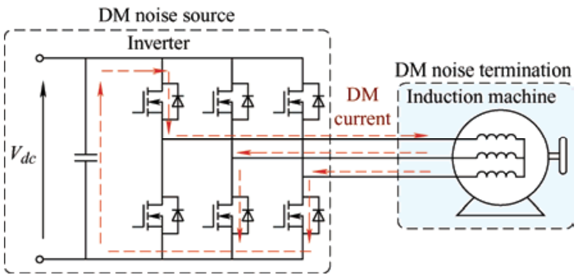

Fig. 1 Propagation path of the DM emission in a typical inverter-fed motor drive system

To facilitate this study, a transmission line model of the induction motor is adopted so that the motor DM impedance under different stator winding faults can be easily determined. In general, there are two types of electrical models for an induction motor: the lumped circuit model [21-24] and transmission line model [25-28]. The lumped circuit model is commonly used to estimate the motor drive overvoltage and EMI noise emission; however, it fails to provide detailed electrical information of each turn of the stator winding [29]. Hence, it lacks the ability to estimate the motor impedance under various stator winding faults. To overcome this limitation, a transmission line model was adopted by treating the stator windings as distributed electrical parameters. The EMI frequency range is usually on the order of tens of kilohertz to tens of megahertz, and within this frequency range, the influence of motor speed and load level on the DM impedance of the motor is negligible [29].

Once the model of the stator winding is constructed, a test setup is proposed to evaluate the impact of stator winding faults on the mode transformation. The DM-to-CM transformation has been well reported[16]; therefore, this study focused on the CM-to-DM transformation. Using a 5.5 kW induction motor as a case study, it was demonstrated that even early-stage stator winding faults can have non-negligible effects on DM noise.

The remainder of this paper is organized as follows. Section 2 describes the comprehensive transmission line model of the induction motor. Section 3 presents the estimation and quantification of the influence of stator winding faults on the motor DM impedance based on the transmission line model, in which the developed model is experimentally validated. Section 4 describes the proposed test setup to evaluate the CM-to-DM transformation caused by stator winding faults and its impact on DM noise emission. Finally, Section 5 concludes the paper.

2 Transmission line model

Fig. 2 shows the transmission line model per unit length (PUL), which was derived from the conventional PUL RLGC (R for resistance, L for inductance, G for conductance and C for capacitance) model shown in Fig. 3 [28]. Additional circuit parameters were included to capture high-frequency behaviors. In the model, L_{lf} and L_{hf} represent the leakage inductances in the low-frequency and high-frequency regions, respectively. R_{sw} denotes the resistive characteristic of the stator winding, considering the skin effect and eddy current losses. C_{iw} captures the capacitive coupling effects between coils in a slot. C_{sf} and R_{sf} represent the capacitance and resistive loss between the stator winding and the motor frame, respectively.

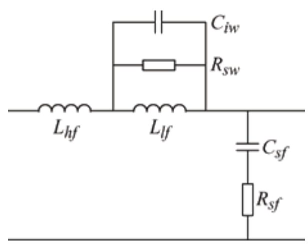

Fig. 2 Transmission line model per unit length

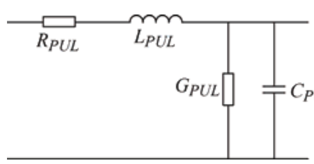

Fig. 3 Conventional PUL RLGC model

The circuit parameters presented in Fig. 2 can be determined based on the scattering (S) parameter measurements of each phase using a vector network analyzer (VNA), as shown in Fig. 4.

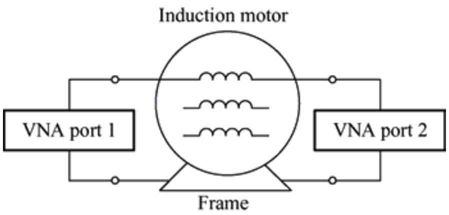

Fig. 4 S-parameter measurement for each phase of motor

Each phase of the motor under test (TECO 1071033064C-1, 3 phases, 5.5 kW, 6-pole) can be considered as a two-port network, and a VNA (Bode 100) is chosen for the S parameter measurement. Based on the measured S parameters, the propagation constant (γ) and characteristic impedance (Z_c) can be determined as follows [30]

$$\gamma=\frac{1}{N}\cosh^{-1}\frac{\left(1+S_{11}\right)\left(1-S_{11}\right)+S_{12}S_{21}}{2S_{21}} \tag{1}$$

$$Z_c=\pm Z_0\sqrt{\frac{\left(1+S_{11}\right)\left(1+S_{22}\right)-S_{12}S_{21}}{\left(1-S_{11}\right)\left(1-S_{22}\right)-S_{12}S_{21}}} \tag{2}$$

where Z_0 is the reference port impedance and N is the number of turns per phase of the stator winding. For the given motor, N=288. Both γ and Z_c in Eq. (1) and Eq. (2) can give rise to several possible solutions, and physically reasonable values are selected based on the criterion described in Ref. [28]. The next step is to extract the PUL RLGC parameters presented in Fig. 2, which were determined using Eqs. (3)-(6).

$$R_{PUL}=\Re(\gamma\cdot Z_c) \tag{3}$$

$$L_{PUL}=\frac{\Im(\gamma\cdot Z_c)}{2\pi f} \tag{4}$$

$$G_{PUL}=\Re(\gamma/Z_c) \tag{5}$$

$$C_{PUL}=\frac{\Im(\gamma/Z_c)}{2\pi f} \tag{6}$$

where $\Re()$ and $\Im()$ represent the real part and imaginary part functions, respectively.

Based on Eqs. (3)-(6), the PUL RLGC parameters for each phase of the induction motor can be extracted. For illustrative purposes, Fig. 5 shows the extracted results for one phase of the motor under testing. Finally, the values of the circuit parameters of the transmission line model shown in Fig. 2 can be determined based on a qualitative analysis of the PUL RLGC parameters. The detailed process of qualitative analysis is described in Ref. [28], and will not be repeated here. Tab. 1 lists the values of the circuit parameters of the transmission line model of the motor under testing.

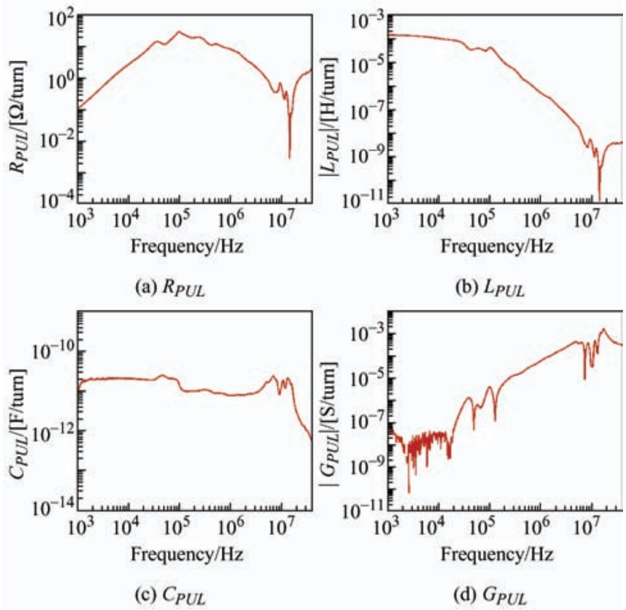

Fig. 5 Extracted PUL RLGC parameters of Phase A of the motor under test

Tab. 1 Circuit parameters of the transmission line model of the motor under test

Circuit parameter	Value		
	Phase A	Phase B	Phase C
L_{lf}/μH	178.1	172.4	168.9
L_{hf}/nH	4.3	4.2	4.5
R_{sw}/Ω	27.6	27.4	26.7
C_{iw}/nF	28.4	30.2	29.5
C_{sf}/pF	15.0	14.8	14.7
R_{sf}/Ω	465.4	475.1	470.3

For verification, the DM impedance between Phases A and B-C of the motor under testing was reproduced based on the obtained circuit parameters, motor winding connection (star connection), and total number of turns (N=288). As shown in Fig. 6, the simulated DM impedance agreed well with the measured DM impedance.

It is worth noting that the DM impedance has an inductive nature at low frequencies because of the winding inductance. After an observed resonance at 15.3 kHz, it becomes capacitive as the frequency increases, owing to the stray capacitance between the stator windings. After the sanity check, the transmission line model was applied to evaluate and quantify the impacts of various stator winding faults on the motor DM impedance.

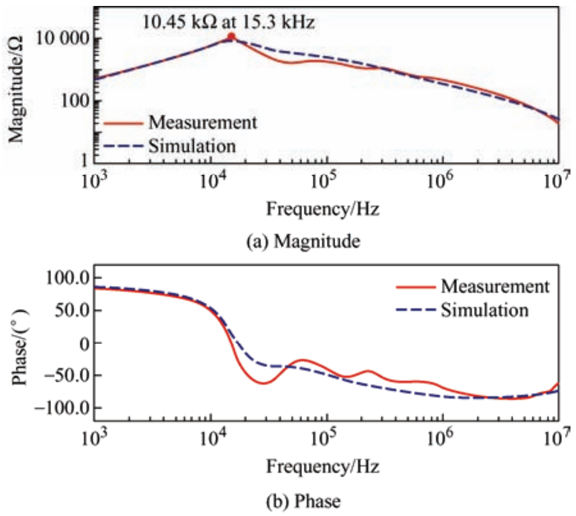

Fig. 6 Measured and simulated DM impedances of the healthy motor under test

3 Impact of stator winding faults on motor DM impedance

3.1 Fault emulation

Fig. 7 shows the stator winding configuration of the motor under testing, where the faults are emulated by removing the respective tapping points of the windings and motor frame. For the turn-to-turn fault, the taps from Phase A with turn numbers 24 and 34 (i.e., A24 and A34) were shorted with a 1-Ω resistor [31]. Phase-to-phase faults with varying severity levels were emulated by shortening the turns A24-B120 and B120-C120. Similarly, the phase-to-ground fault was emulated by shortening the taps for turn A24 and motor frame G.

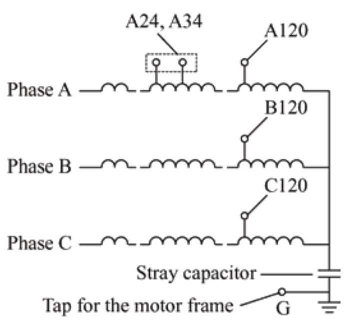

Fig. 7 Stator winding configuration of the motor under test

To emulate the stator winding faults (i.e., turn-to-turn, phase-to-phase, and phase-to-ground faults), the respective tapping points of the windings and motor frame should be shorted with a small-value resistor. Meanwhile, the resistor should be able to limit the short-circuit current to avoid destruction of the induction motor when a voltage source is used to power the shorted motor. The 1-Ω resistor was used for these purposes [31-32].

3.2 Measured motor DM impedance under stator winding faults

A stator winding fault due to low-impedance contact between the shorted turns or phases can lead to changes in the DM impedance of the motor, as well as the resultant DM noise emission. The solid lines in Figs. 8a-8d show the measured motor DM impedances between Phases A and B-C under various stator winding faults. The first resonant frequency of the measured impedance and the variation in the impedance value were selected as indicators of winding faults [18, 33]. As observed in Fig. 8a, the emulated turn-to-turn fault (A24-A34 short) reduces the DM impedance by 10% at the resonant frequency, which can cause higher DM noise emission and can be a potential EMI issue.

The insulation breakdown between the two phases is a more severe fault, because the high voltage difference between these phases can lead to irreversible damage after a period of time. However, in a three-phase balanced motor, the voltage difference between the windings near the neutral point can be small, and an incipient phase-to-phase fault may not immediately affect the operation of the motor. As shown in Fig. 8b, the phase-to-phase fault (A24-B120 short) decreases the DM impedance significantly and results in a shift of the resonant frequency from 15.3 kHz to 33.9 kHz. In contrast, another phase-to-phase fault (B120-C120 short) has a relatively small impact on the DM impedance, as shown in Fig. 8c. This is expected because B120 and C120 are the two equipotential points when the DM impedance is measured between Phase A and B-C.

In an ungrounded insulated terrestrial system, such as hospital operating rooms and naval ships, all three live phases float, and there is no closed loop for a line-frequency current to flow at a single phase-to-ground fault [19]. Hence, the influence of phase-to-ground faults on DM impedance is worth investigating in these scenarios. It is observed in Fig. 8d that the phase-to-ground fault (A24-G short) leads to a lower DM impedance along with a downwards shift of resonant frequency from 15.3 kHz to 7.1 kHz.

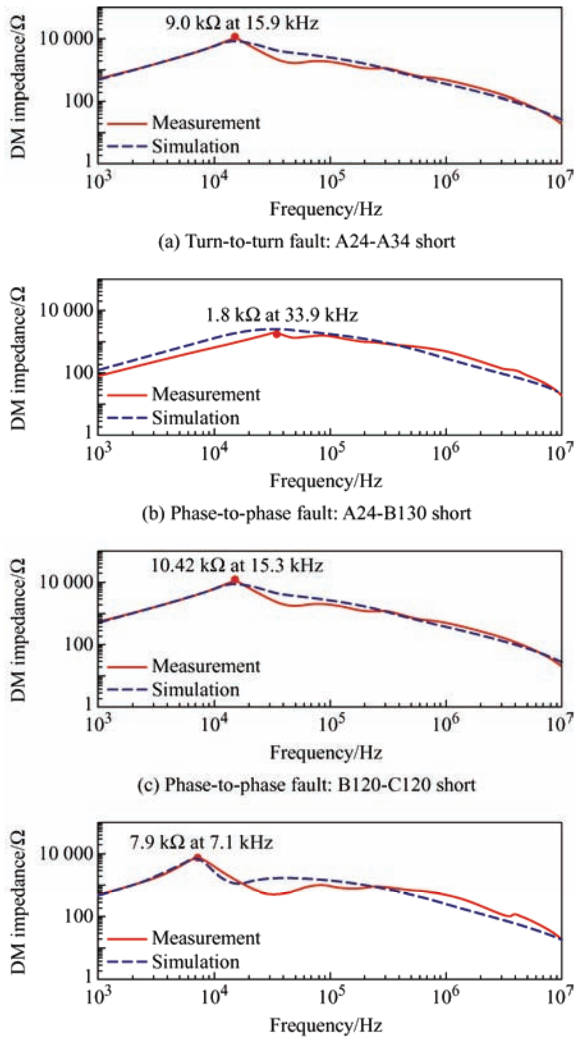

(a) Turn-to-turn fault: A24-A34 short

(b) Phase-to-phase fault: A24-B130 short

(c) Phase-to-phase fault: B120-C120 short

(d) Phase-to-ground fault: A24-G short

Fig. 8 Measured (solid line) and simulated (dashed line) motor DM impedances between Phase A and Phase B-C under various fault conditions

3.3 Simulated motor DM impedance under stator winding faults

Using the PUL model presented in Fig. 2, together with the motor winding connection, the total number of turns, and the fault type and location, a 3-phase transmission line model of the motor under stator winding faults can be constructed, as shown in Fig. 9. For the motor under testing (TECO 1071033064C-1, 3 phases, 5.5 kW, 6-pole), the values of the circuit

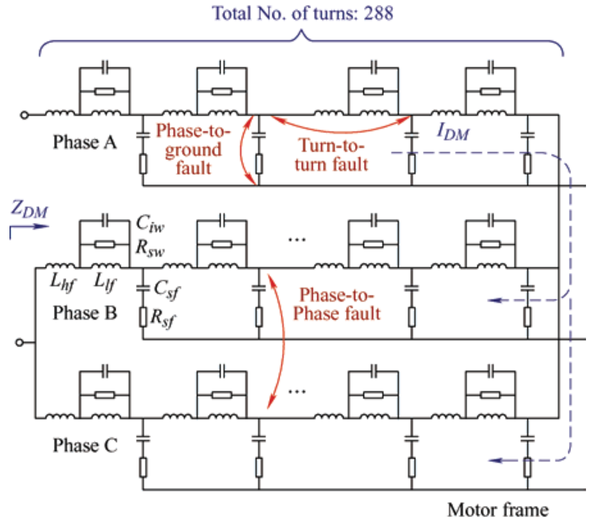

Fig. 9 Three-phase transmission line model of the star-connected induction motor under stator winding faults

parameters of the transmission line model are presented in Tab. 1. In addition, the motor is configured in a star connection, and there are 288 subsections in each phase to represent each turn of the stator winding. To be consistent with the emulated stator winding faults in the experimental setup, the simulated stator winding faults were also created by shortening the respective tapping points of the windings and the motor frame with a 1-Ω resistor [31-32]. Finally, the motor DM impedance between Phases A and B-C. The simulated motor DM impedances for the above-mentioned four stator winding faults (i.e., A24-A34 short, A24-B130, B120-C120 short, and A24-G short) are plotted in Figs. 8a-8d with dashed lines. It can be observed that the simulated results for each stator winding fault show relatively good agreement with the measured results.

Some deviations in certain frequency regions are expected because the model assumes that the high-frequency coil parameters are evenly distributed along the stator winding. In reality, these parameters are not evenly distributed, owing to layout differences and manufacturing tolerance [34]. Nevertheless, the model demonstrates reasonable agreement with the measured results for various faults.

4 CM-to-DM transformation

The stator winding faults not only change the motor DM impedance but also introduce an imbalance between the stator windings in different phases. This can result in DM-to-CM EMI transformation and vice versa [35]. It has been reported that the CM-to-DM transformation is more pronounced than the DM-to-CM transformation for a given amplitude or phase mismatch [36]. Both CM and DM EMI filters in a motor drive system are usually designed assuming perfect mode separation, because of the difficulty in quantifying mode transformation in different applications [37]. Hence, it is worthwhile to investigate the CM-to-DM transformation caused by stator winding faults and its resultant influence on DM noise emission.

Figs. 10a and 10b show the test setup to evaluate the mode transformation, where a CM voltage source is applied to the induction motor by shortening Phases A, B, and C. The CM voltage source was a square wave with an amplitude of 10 V and a switching frequency of 10 kHz, which was generated by a MOSFET half-bridge (EVAL-1EDC20H12AH-SIC) with a controller (TMS320F28379D), as illustrated in Fig. 11.

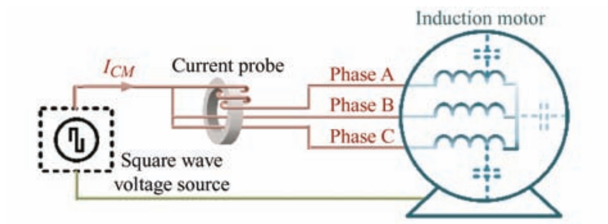

(a) Schematic diagram

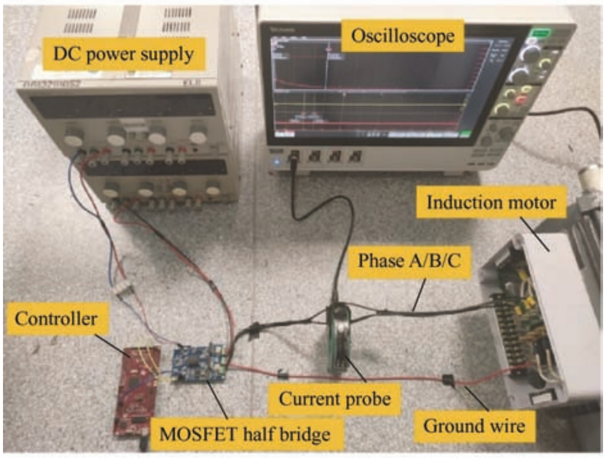

(b) Photograph

Fig. 10 Proposed test setup to measure the CM-to-DM transformation

To evaluate the CM-to-DM transformation, the DM current was monitored with a high-frequency current probe (Pearson 6600) and a spectrum analyzer (Tektronix MSO54 oscilloscope operating in the spectrum analyzer function) using the configuration shown in Fig. 10a, which yields

$$I_{DM\text{-}A}=\frac{1}{3}(2i_a-i_b-i_c) \tag{7}$$

where $I_{DM\text{-}A}$ is the DM current for Phase A. Ideally, $I_{DM\text{-}A}$ should be zero for a perfectly balanced system, as the DM noise source is not presented in the circuit. However, an imbalance exists, thus the DM current is finite.

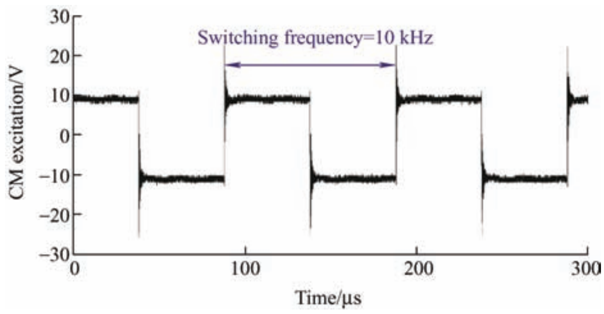

Fig. 11 Waveform of the CM excitation

Fig. 12 shows the DM emission versus the frequency induced by the CM excitation for the above-mentioned stator winding faults. The horizontal axis is expressed in terms of the harmonic order to clearly demonstrate the mode transformation. The inherent asymmetry caused by manufacturing tolerances is inevitable in a motor drive system [38]; thus, finite DM emissions exists even for a healthy motor without any stator winding faults. The DM emission measured under the healthy conditions was used as a reference to evaluate the CM-to-DM transformation caused by the stator winding faults.

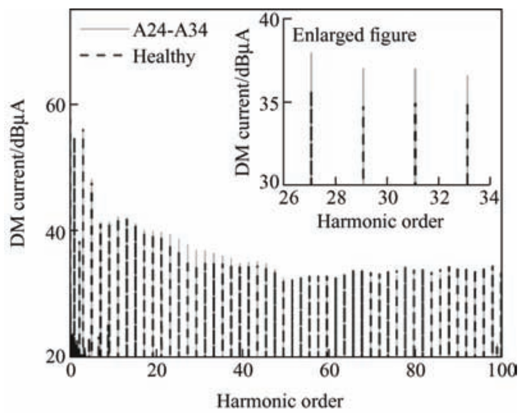

(a) Turn-to-turn fault A24-A34

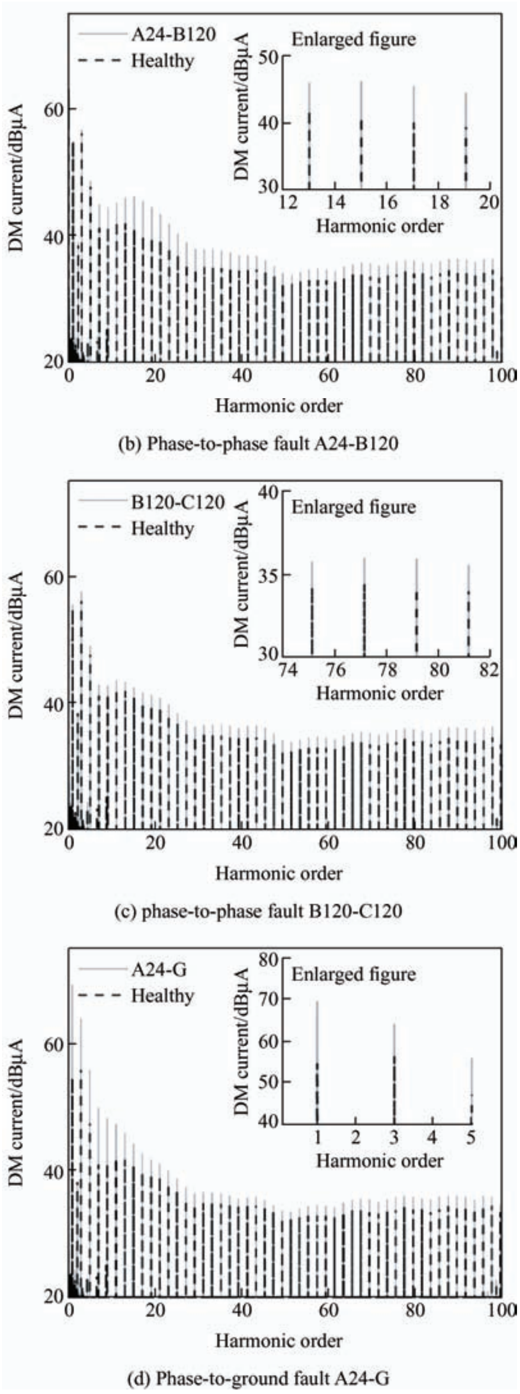

Fig. 12 Comparison between $I_{DM\text{-}A}$ at healthy condition and at fault condition

As shown in Fig. 12, the DM emission increases with the severity of the stator winding faults. As illustrated in the enlarged images in the figures, the highest increment in the DM noise emissions occurs at the phase-to-ground fault, which registers an increase of 14.7 dB.

5 Conclusions

In this study, the influence of stator winding faults on motor DM impedance and CM-to-DM mode transformation was investigated and quantified. By adopting a transmission line model of the induction motor, the change in the motor DM impedance under various stator winding faults can be predicted with good accuracy. In addition, a test setup was developed to evaluate the impact of stator winding faults on the CM-to-DM transformation. The results demonstrate that even early-stage stator winding faults can result in noticeable changes in DM noise. Future research will explore feasible and efficient methods based on the DM impedance and DM noise for the online detection of stator winding faults with different types, severities, and locations.

References

[1] S Yin, Y Liu, Y Liu, et al. Comparison of SiC voltage source inverters using synchronous rectification and freewheeling diode. *IEEE Trans. Ind. Electron.*, 2018, 65(2): 1051-1061.

[2] Z Fang, D Jiang, Y Zhang. Study of the characteristics and suppression of EMI of inverter with SiC and Si devices. *Chinese Journal of Electrical Engineering*, 2018, 4(3): 37-46.

[3] A Moeini, S Wang. A DC link sensor-less voltage balancing technique for cascaded H-bridge multilevel converters with asymmetric selective harmonic current mitigation-PWM. *IEEE Trans. Power Electron.*, 2018, 33(9): 7571-7581.

[4] S Jiang, Y Liu, Z Mei, et al. A magnetic integrated LCL-EMI filter for a single-phase SiC-MOSFET grid-connected inverter. *IEEE J. Emerg. Sel. Topics Power Electron.*, 2020, 8(1): 601-617.

[5] S Wang, Y Y Maillet, F Wang, et al. Investigation of hybrid EMI filters for common-mode EMI suppression in a motor drive system. *IEEE Trans. Power Electron.*, 2010, 25(4): 1034-1045.

[6] F Luo, S Wang, F Wang, et al. Analysis of CM volt-second influence on CM inductor saturation and design for input EMI filters in three-phase DC-fed motor drive systems. *IEEE Trans. Power Electron.*, 2010, 25(7): 1905-1914.

[7] Y Liu, K Y See, K J Tseng. Conducted EMI prediction of the PFC converter including nonlinear behavior of boost inductor. *IEEE Trans. Electromagn. Compat.*, 2013, 55(6): 1107-1114.

[8] S J Rind, Y Ren, Y Hu, et al. Configurations and control

of traction motors for electric vehicles: A review. *Chinese Journal of Electrical Engineering*, 2017, 3(3): 1-17.

[9] Y Liu, H Wang, G Wang, et al. Reduced EMI noise with the consideration of magnetic material design in the grid-connected inverter for more electric aircraft. *Proc. IEEE Int. Magn. Conf.*, Singapore, IEEE, 2018: 1-2.

[10] H Chen, T Wang. Estimation of common-mode current coupled to the communication cable in a motor drive system. *IEEE Trans. Electromagn. Compat.*, 2018, 60(6): 1777-1785.

[11] W Chen, X Yang, Z Wang. A novel hybrid common-mode EMI filter with active impedance multiplication. *IEEE Trans. Ind. Electron.*, 2011, 58(5): 1826-1834.

[12] D Jiang, P Ning, R Lai, et al. Modular design method for motor drives. *Chinese Journal of Electrical Engineering*, 2018, 4(1): 1-10.

[13] H Chen, J Wu, X Zheng. Elimination of common-mode choke saturation caused by self-resonance of the EMI filter in a variable-frequency drive system. *IEEE Trans. Electromagn. Compat.*, 2019, 61(4): 1226-1233.

[14] Y Zhang, Q Li, D Jiang. A motor CM impedance based transformerless active EMI filter for DC-side common-mode EMI suppression in motor drive system. *IEEE Trans. Power Electron.*, 2020, 35(10): 10238-10248.

[15] Z Zhang, Y Hu, X Chen, et al. A review on conductive common-mode EMI suppression methods in inverter fed motor drives. *IEEE Access*, 2021, 9: 18345-18360.

[16] F Fan, Z Zhao, P Tu, et al. Impact of motor stator winding faults on common-mode current. *Proc. Asia-Pacific Symp. Electromagn. Compat. (APEMC)*, Nusa Dua-Bali, Indonesia, IEEE, 2021: 1-4.

[17] P F Albrecht, J C Appiarius, R M McCoy, et al. Assessment of the reliability of motors in utility applications-updated. *IEEE Trans. Energy Convers.*, 1986, EC-1(1): 39-46.

[18] Z Zhao, F Fan, W Wang, et al. Detection of stator interturn short-circuit faults in inverter-fed induction motors by online common-mode impedance monitoring. *IEEE Trans. Instrum. Meas.*, 2021, 70: 3513110.

[19] P V Vugt, R Bijman, R B Timens, et al. Impact of grounding and filtering on power insulation monitoring in insulated terrestrial power networks. *Proc. Int. Symp. Electromagn. Compat.*, Brugge, Belgium, IEEE, 2013: 472-477.

[20] H Bishnoi, P Mattavelli, R Burgos, et al. EMI behavioral models of DC-fed three-phase motor drive systems. *IEEE Trans. Power Electron.*, 2014, 29(9): 4633-4645.

[21] A F Moreira, T A Lipo, G Venkataramanan, et al. High-frequency modeling for cable and induction motor overvoltage studies in long cable drives. *IEEE Trans. Ind. Appl.*, 2002, 38(5): 1297-1306.

[22] B Mirafzal, G L Skibinski, R M Tallam. Determination of parameters in the universal induction motor model. *IEEE Trans. Ind. Appl.*, 2009, 45(1): 142-151.

[23] D Lindenthaler, G Brasseur. Signal-bandwidth evaluation for power measurements in electric automotive drives. *IEEE Trans. Instrum. Meas.*, 2015, 64(6): 1336-1343.

[24] G Vidmar, D Miljavec. A universal high-frequency three-phase electric-motormodel suitable for the delta- and star-winding connections. *IEEE Trans. Power Electron.*, 2015, 30(8): 4365-4376.

[25] W R Eisenstadt, Y Eo. S-parameter-based IC interconnect transmission line characterization. *IEEE Trans. Compon., Hybrids, Manuf. Technol.*, 1992, 15(4): 483-490.

[26] D Zhao, G Rietveld, G M Teunisse. A multistep approach for accurate permittivity measurements of liquids using a transmission line method. *IEEE Trans. Instrum. Meas.*, 2011, 60(7): 2267-2274.

[27] H De Gersem, A Muetze. Finite-element supported transmission-line models for calculating high-frequency effects in machine windings. *IEEE Trans. Magn.*, 2012, 48(2): 787-790.

[28] Y Ryu, B R Park, K J Han. Estimation of high-frequency parameters of AC machine from transmission line model. *IEEE Trans. Magn.*, 2015, 51(3): 8101404.

[29] B Mirafzal, G L Skibinski, R M Tallam, et al. Universal induction motor model with low-to-high frequency-response characteristics. *IEEE Trans. Ind. Appl.*, 2007, 43(5): 1233-1246.

[30] Y Ryu, K J Han. Improved transmission line model of the stator winding structure of an AC motor considering high-frequency conductor and dielectric effects. *Prof. Int. Electr. Mach. Drives Conf. (IEMDC)*, Miami, FL, USA, IEEE, 2017: 1-6.

[31] F R Blánquez, C A Platero, E Rebollo, et al. Evaluation of the applicability of FRA for inter-turn fault detection in stator windings. *Prof. Int. Symp. Diag. Elec. Mach., Power Electron. Drives (SDEMPED)*, Valencia, Spai, IEEE, 2013: 177-182.

[32] C C Yeh, G Y Sizov, A Sayed-Ahmed, et al. A reconfigurable motor for experimental emulation of stator

winding interturn and broken bar faults in polyphase induction machines. *IEEE Trans. Energy Convers*., 2008, 23(4): 1005-1014.

[33] M Subramanian. Detection of winding inter-turn faults: Detection based on frequency response analysis-Part I. *Transformer Mag*., 2020, 7(1): 112-118.

[34] G Suresh, A Toliyat, A Rendusara, et al. Predicting the transient effects of PWM voltage waveform on the stator windings of random wound induction motors. *IEEE Trans. Power Electron*., 1999, 14(1): 23-30.

[35] S Wang, F C Lee. Investigation of the transformation between differential-mode and common-mode noises in an EMI filter due to unbalance. *IEEE Trans. Electromagn. Compat*., 2010, 52(3): 578-587.

[36] P S Niklaus, M M Antivachis, D Borti, et al. Analysis of the influence of measurement circuit asymmetries on three-phase CM/DM conducted EMI separatio. *IEEE Trans. Power Electron*., 2021, 36(4): 4066-4080.

[37] P S Chen, Y S Lai. Effective EMI filter design method for three-phase inverter based upon software noise separation. *IEEE Trans. Power Electron*., 2010, 25(11): 2797-2806.

[38] V Nguyen, D Wang, J Seshadrinath, et al. A method for incipient interturn fault detection and severity estimation of induction motors under inherent asymmetry and voltage imbalance. *IEEE Trans. Transport. Electrific*., 2017, 3(3): 703-715.

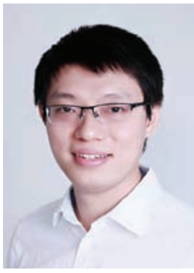

Fei Fan (M'19) received the B.Eng. degree in Electrical Engineering from Tianjin University, Tianjin, China, in 2014, and the M.Sc. in Power Engineering and Ph.D. degrees in Electrical Engineering from Nanyang Technological University (NTU), Singapore, in 2015 and 2020, respectively.

He is currently a Research Fellow in the School of Electrical and Electronic Engineering, NTU. His research interests are electromagnetic compatibility and electromagnetic interference measurement, in-circuit impedance extraction, and EMI filter design for motor-drive system.

Dr. Fan was a recipient of the Best Student Paper Award at the 2017 Asia-Pacific Symposium on Electromagnetic Compatibility (APEMC) and Progress in Electromagnetics Research Symposium (PIERS).

Zhenyu Zhao (M'21) received the B.Eng. degree in Electrical Engineering from Huazhong University of Science and Technology, Wuhan, China, in 2015, and the M.Sc. in Power Engineering and Ph.D. degrees in Electrical Engineering from Nanyang Technological University, Singapore, in 2016 and 2021, respectively.

He is currently a Research Fellow in the Schaeffler Hub for Advanced Research, Nanyang Technological University. His research interests include electromagnetic compatibility (EMC), electromagnetic sensors, impedance measurement, and health monitoring. In these areas, he has authored and co-authored more than 40 refereed technical papers.

Dr. Zhao was a recipient of the Best Student Paper Award at the 2018 Joint IEEE International Symposium on Electromagnetic Compatibility & Asia-Pacific Symposium on Electromagnetic Compatibility (Joint IEEE EMC & APEMC), the Best Paper Award Finalists at the 2021 APEMC. He was nominated and invited to participate in the Global Young Scientists Summit (GYSS) in 2019 and 2022. He has served as a Session Chair and a TPC Member for several international conferences. Since 2022, he has been serving as the Secretary for IEEE EMC Society Singapore Chapter.

Huamin Jie (S'22) received the B.Eng. degree in Electrical Engineering from Wuhan University, Wuhan, China, in 2019, and the M.Sc. degree in Power Engineering from Nanyang Technological University, Singapore, in 2020, respectively. He is currently working toward the Ph.D. degree with the School of Electrical and Electronic Engineering, Nanyang Technological University.

His research interests include impedance measurement, device modeling, electromagnetic interference (EMI), and EMI filter design.

Quqin Sun received the B.Eng. and Ph.D. degrees in Electrical Engineering from Huazhong University of Science and Technology, Wuhan, China. in 2011 and 2016, respectively.

He worked as a Research Associate at the Institute of Fluid Physics of China Academy of Engineering Physics till 2018. From 2018 to 2021, he joined Nanyang Technological University, Singapore as a Research Fellow. He is now an Engineer in Wuhan Second Ship Design and Research Institute. His research interest spans within high-field pulsed magnet design, electromagnetic launch, laser-ultrasonic non-destructive inspection and motor condition monitoring.

Pengfei Tu received the B.Eng. degree in Electrical Engineering from Wuhan University, Wuhan, China, in 2013, and the M.Sc. and Ph.D. degrees in Power Engineering from Nanyang Technological University, Singapore, in 2014 and 2019, respectively.

He is currently a Research Fellow in the School of Electrical and Electronic Engineering, Nanyang Technological University. His current research interests include reliability of multilevel converters, model predictive control, wireless power transfer and energy management system.

Zhou Shu (M'21) received the B.Sc., M.Eng. and Ph.D. degrees in Integrated Circuit and System from Chongqing University, Chongqing, China, in 2015, 2017, and 2020, respectively.

In 2021, he joined Nanyang Technological University, Singapore, as a Research Fellow. His research interest includes mixed-signal Integrated circuit design for high-speed wireline links, power management unit and low-power sensor interfaces, and testing and fault diagnosis for industrial applications.

Wensong Wang (M'18-SM'22) received the Ph.D. degree in Communication and Information Systems from Nanjing University of Aeronautics and Astronautics, Nanjing, China, in 2016.

From 2013 to 2015, he was a Visiting Scholar with the University of South Carolina, Columbia, USA. In 2017, he joined Nanyang Technological University, Singapore, as a Research Fellow, and now he is a Senior Research Fellow.

His research interests include MIMO antenna, antenna array and advanced sensors.

Kye Yak See (M'86-SM'02) received the B.Eng. degree in Electrical Engineering from National University of Singapore, Singapore, in 1986, and the Ph.D. degree in Electrical Engineering from Imperial College London, UK, in 1997.

From 1986 and 1991, he was with Singapore Technologies Electronics, Singapore, as a Senior Engineer. From 1991 to 1994, he was a lead Design Engineer with ASTEC Custom Power, Singapore. Since 1997, he has been with Nanyang Technological University (NTU), Singapore, as a Faculty Member. He is currently an Associate Professor with the School of Electrical and Electronic Engineering, NTU. He holds concurrent appointment as Director of the Electromagnetic Effects Research Laboratory and Director of SMRT-NTU Smart Urban Rail Corporate Laboratory. His current research interests are electromagnetic compatibility (EMC), signal integrity and real-time condition monitoring.

Dr. See was the Founding Chairs of the IEEE Electromagnetic Compatibility (EMC) Chapter, IEEE Aerospace and Electronic Systems, and the IEEE Geoscience and Remote Sensing Joint Chapter in Singapore. He was the General Chairs of 2015 Asia Pacific Conference on Synthetic Aperture Radar (APSAR 2015) and 2018 International Conference on Intelligent Rail Transportation (ICIRT 2018). Since January 2012, he has been the Technical Editor of the IEEE Electromagnetic Compatibility Magazine.